Engineering Optimization

ISSN: (Print) (Online) Journal homepage: https://www.tandfonline.com/loi/geno20

A simple density filter for the topology optimization of coated structures

Bing Yi, Gil Ho Yoon & Xiang Peng

To cite this article: Bing Yi, Gil Ho Yoon & Xiang Peng (2021) A simple density filter for the topology optimization of coated structures, Engineering Optimization, 53:12, 2088-2107, DOI: 10.1080/0305215X.2020.1845326

To link to this article: https://doi.org/10.1080/0305215X.2020.1845326

Published online: 25 Nov 2020.

ENGINEERING OPTIMIZATION
2021, VOL. 53, NO. 12, 2088–2107
https://doi.org/10.1080/0305215X.2020.1845326

Taylor & Francis
Taylor & Francis Group

A simple density filter for the topology optimization of coated structures

Bing Yi[a], Gil Ho Yoon[b] and Xiang Peng[c]

[a]School of Traffic and Transportation Engineering, Central South University, Changsha, People's Republic of China; [b]School of Mechanical Engineering, Hanyang University, Seoul, South Korea; [c]Key Laboratory of E&M, Zhejiang University of Technology, Hangzhou, People's Republic of China

ABSTRACT

Coated structures are structures with a solid thin-walled coating enclosing substrates. Coated structures with porous substrates (infills) are often adopted in additive manufacturing to reduce the material cost and printing time, while improving robustness against local bucking, unknown loads and material deficiencies. This article presents a new density filter method for the topology optimization of coated structures. Compared to previous work, the new method uses only the density filter and its projection, and does not rely on the gradient of the density field, which can pose a numerical challenge in large-scale problems. Since the output of the proposed density filter is bounded exactly between zero and one, it will also eliminate the need to approximate the maximum magnitude of the density gradient, the inaccuracy of which can cause non-uniform thickness of the coating. The proposed filter also realizes a smoother change between substrate material and coating material, and encourages the merging and splitting of coatings during optimization. Several numerical examples on compliance minimization are presented to demonstrate the validity and effectiveness of the proposed density filter.

ARTICLE HISTORY
Received 29 January 2020
Accepted 29 October 2020

KEYWORDS
Topology optimization; coated structure; density filter; PDE filter

1. Introduction

Coating technology has been widely used in industry for substrate structure protection or special functionality improvement (Møller and Nielsen 2013). Recently, coatings have also become instrumental for implementing novel structural concepts. For example, with the help of (coating technology, a structure with automatic functionality called 'smart coating' was constructed to provide a substructure in response to external impacts (Shchukin and Möhwald 2013). Some of the problems with the implementation of complex structures with coatings is their high cost and difficulty of manufacture. By using electrolytic plating, a type of ultralight metallic material (a micro-lattice of nickel phosphorous tubes) was constructed from polymers to form a complex substructure, and nickel on the surface was used as the coating (Schaedler *et al.* 2011). In addition, with the fast progress of 3D printing technology, bone-like structures and hollow-shell structures (both can be called coating structures) inspired by nature can be manufactured easily (Syed *et al.* 2018).

Coating structures are often used in additive manufacturing to reduce material costs and improve manufacturing efficiency (Liu *et al.* 2018; Y. Wang *et al.* 2020). The conventional method uses repetitive regular patterns (*e.g.* triangular, hexagonal or truss structures) for the interior structure with a solid coating structure as the outer. W. Wang *et al.* (2013) introduced a new method for inner

CONTACT Bing Yi bingyi@csu.edu.cn

truss optimization based on sparsity analysis, and the obtained skin-frame structure reduced the amount of material required while guaranteeing physical stability. Lu *et al.* (2014) employed a hollowing optimization method based on the Voronoi diagram to obtain optimal interior tessellation, which has a large strength-to-weight ratio. However, the truss model is limited in its optimization search space, and the non-gradient-based hollowing optimization method is inefficient and uncontrollable. Topology optimization is considered to be a powerful and effective method for lightweight structure optimization in additive manufacturing. Plenty of topology optimization methods, including the homogenization method (Bendsøe and Kikuchi 1988), the density method (Sigmund and Maute 2013), the level-set method (M.Y. Wang, X. Wang, and Guo 2003; Allaire, Jouve, and Toader 2004) and the evolutionary structure optimization method (Xie and Steven 1993), have been studied widely for topology optimization.

Most studies done in the past for topology optimization considered the problem of solid structure (Sigmund and Maute 2013; M.Y. Wang, X. Wang, and Guo 2003; Allaire, Jouve, and Toader 2004; Xie and Steven 1993; Peng *et al.* 2018). Recently, more and more researchers have paid attention to lattice structure optimization (J. Wu *et al.* 2018; Yi *et al.* 2019), which was the original focus for topology optimization with the homogenization method (Bendsøe and Kikuchi 1988). Clausen *et al.* (Clausen, Aage, and Sigmund 2015, 2016) first proposed a method for optimizing coated structures, which used a solid shell as the outer part and an isotropic base material that could be implemented with an inner uniform lattice structure. Following this work, J. Wu *et al.* (J. Wu, Clausen, and Sigmund 2017; J. Wu *et al.* 2018) presented a density-based optimization method with a local volume constraint to design both the coating and the infill structure to minimize the compliance of the structure. Although gradient-norm-based coating structure modelling is clear and easy, the computation of the gradient is complex and exact approximation of the maximum of the gradient norm is very difficult. In the present authors' previous work, a new coating filter for coated structures with a regular mesh was proposed (Yoon and Yi 2019); however, the coating was handled as a manufacturing constraint for substructure protection, and it suffered from the checkerboard pattern problem, which is present in most methods with a regular mesh. Similarly, the level-set-based method was used in an attempt to model coating structures (Y. Wang and Kang 2018) and shell-infill structures (Fu, Li, Gao, *et al.* 2019; Fu, Li, Xiao, *et al.* 2019). Though the modelling of coatings can be done easily with the distance-function-based level set, the design and optimization of a non-uniform inter-infill structure is still a challenging problem.

In the proposed method, an easy and new density filter is proposed for modelling coating structures with irregular meshes, which can avoid the complex computation of the gradient. In addition, the formulation of coated structures is designed to be bounded between zero and one, which overcomes the problem of accurately approximating the maximum gradient norm. Further, the coating formulations can change states smoothly among void, base and coating materials; hence, it is easy to merge isolated coating structures. This article is organized as follows. The details of the new coating filter and the derivation of the shape sensitivity are described in Section 2. Section 3 presents several numerical examples to show the performance of the presented coating filter with topology optimization problems. Section 4 presents the conclusions and suggests some future research topics.

2. Development of a new coating filter

2.1. Material model

The new coating model is composed of two steps, *i.e.* the density filtering procedure and the projection procedure, as shown in Figure 1. In the present density filtering procedure, a combination of the density filter and the modified density filter is employed to render the coating structure. Compared with a previous approach (Clausen, Aage, and Sigmund 2015), gradient computation of the design variables is not employed.

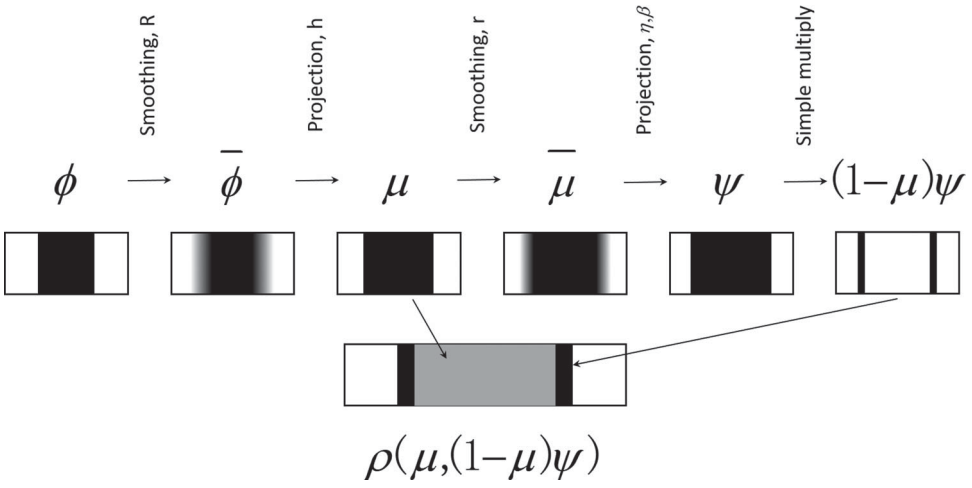

Figure 1. A new density filter for coating structure modelling. $\phi, \overline{\phi} \geq h$ and $\phi, \overline{\phi} \leq -h$ are shown as black and white, respectively; zero and one are shown as black and white for μ, $\overline{\mu}$ and ψ, respectively; coated material, base material and void of the density ρ are shown as black, grey and white, respectively.

2.1.1. New coating structure model

The present approach to the formation of the coating structure is composed of two steps: the filtering procedure and the projection procedure. The filtering procedure is used to construct the base structure, and the second procedure is a simple mathematical procedure that is used to construct the coating layer. As the computation of the density gradient is not accurate and due to the high costs of computation and memory resource, a simple algebraic formation is proposed for the modelling of coating in the present study. The second procedure involves a similar filtering procedure, and the projection processes the original design variable (the base structure). After that, this second procedure combines the density field and the smooth projected density field to model the coating layer. Then, the filtered design variables become bounded between zero and one; this aspect can be regarded as one of the merits of the present approach compared with the other approaches using the gradient of the design variables. The overall description of the proposed coating scheme is illustrated in Figure 1.

First, the design variable ϕ is smoothed with the neighbourhood radius R to get $\overline{\phi}$, and then Heaviside projection is used to get μ, which is the density field. Following the first step, a similar smoothing filter with a different neighbourhood radius r is used to smooth the density field, and then the projection method (Guest, Prévost, and Belytschko 2014) is used to get ψ. Finally, the coating structure is formed by simply multiplying ψ by $1 - \mu$. The thickness of the coating is easily controlled by setting the filter radius r of the filtering of the density field μ.

As the present approach uses simple algebra for the filtered design variables and the design variable, it does not require computation of the gradient or approximation of the maximum of the gradient norm. Furthermore, another issue in topology optimization taking the coating into consideration is the smooth transition of the void or base material to the coating layers. This aspect is crucial for the merging of holes with coating layers. For the state change in the boundary between base structures and void parts, the gradient-based coating and the proposed new coating perform in the same way. However, in the design domain with the density field, the proposed method is chosen over the gradient method owing to its ability to change smoothly from base structure to coating and vice versa.

This characteristic plays an important role in merging isolated coating structures and holes during the topology optimization process. For example, the initialization of the base material for topology optimization with $\rho = 0.5$ in the middle domain and $\rho = 0$ at the outside domain is shown in Figure 2(a). The coated formulation of Clausen, Aage, and Sigmund (2015) is shown in Figure 2(b).

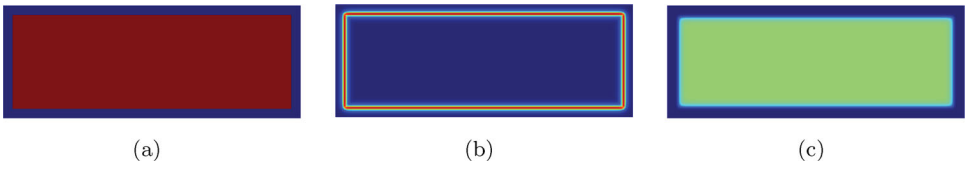

Figure 2. Illustration of the material state at the boundary and inside the design domain: (a) the density of the base material; (b) the gradient-based coating; and (c) the new coating. (For interpretation of the references to colour in this figure, the reader is referred to the web version of this article.)

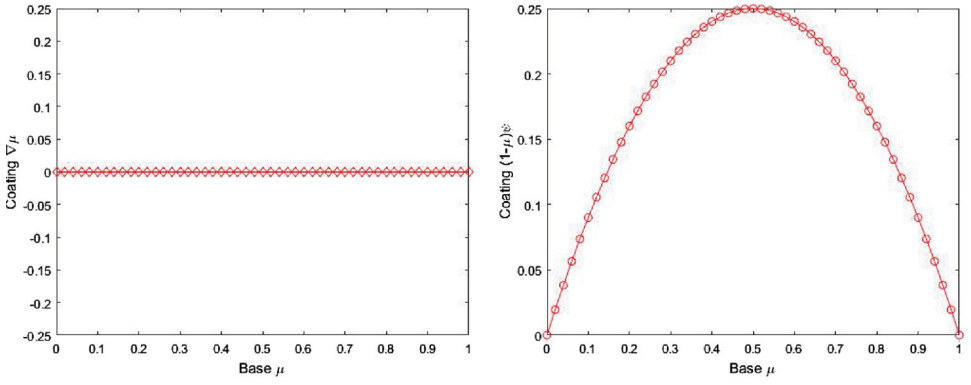

Figure 3. Illustration of the material state change inside the design variable: (a) the gradient-based coating; and (b) the new coating.

It only has coating at the boundary between the inside and outside domains, and with the topology optimization procedure going on, it would perform similarly by putting coated material on the boundary of the base materials. Figure 2(c) shows the coating material of the proposed method. It is obvious that the proposed method can model both base and coated materials together in the design domain, and the optimization will determine the arrangement of the base material and the coated material. Figure 3 shows the change in material state inside the design domain by changing the design variable (the density of the base material). It can be easily seen that the gradient of the density field is always zero inside the density field, as it is uniform, as shown in Figure 3(a). Hence, it is difficult to change the state of materials from base material to coated material directly inside the material domain, and it can only create holes (void material) inside it and then put the coating on the boundary of the hole. However, the new coating modelling shown in Figure 3(b) changes smoothly while the density field changes; hence, it can create coating inside the base structure and can also merge isolated coating in the density field by using an appropriate threshold for projection.

Figure 4 shows a coating structure optimization example—the Messerschmitt–Bölkow–Blohm (MBB) beam—with holes merging by using the proposed method. The design variable ϕ is initialized with -1 in the hole and 1 for the other part in the design domain. It changes smoothly at the interface, which can be modelled as the coating structure, as shown in Figure 4(a) in black. The holes with coating merge with iterations using the gradient-based optimization method, as shown in the upper left and right parts of Figures 4(b)–4(d) and also the middle part of Figures 4(c)–4(h). The proposed method also can merge island holes, as shown in the top middle part of Figures 4(e) and 4(f). Figures 4(h) and 4(i) show that the proposed method can merge more holes during the optimization if necessary. Finally, a sample structure is obtained with the coating on the surface of the base material.

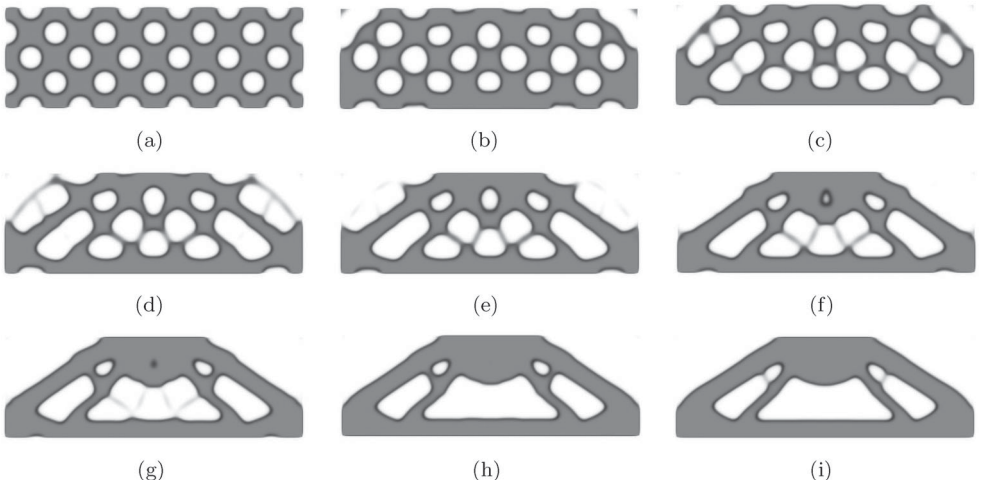

Figure 4. Hole evolution in the MBB beam example with non-uniform initialization: (a) first iteration; (b) 14th iteration; (c) 28th iteration; (d) 33rd iteration; (e) 37th iteration; (f) 42nd iteration; (g) 46th iteration; (h) 52nd iteration; (i) 79th iteration.

The following subsections describe the details of the above considerations.

2.1.2. Filters

To handle the checkerboard problem and get an independent mesh result, the Helmholtz partial differential equation (PDE) filter (Lazarov and Sigmund 2011; Kawamoto *et al.* 2011) was adopted for filtering both the design variable ϕ and the density field μ with different neighbourhood radii.

The Helmholtz PDE filter for the design variable $\phi \in [-1, 1]$ can be expressed as

$$-R^2\nabla^2\overline{\phi} + \overline{\phi} = \phi, \tag{1}$$

where R denotes the neighbourhood radius for controlling the smallest length scale feature.

Similarly, the filtering for the density field $\mu \in [0, 1]$ can be formulated as

$$-r^2\nabla^2\overline{\mu} + \overline{\mu} = \mu, \tag{2}$$

where r is used to manage the thickness of the coating structure. The relation between R, r and the filter radii R_s, r_s using standard filtering techniques can be expressed as

$$R = \frac{R_s}{2\sqrt{3}}, \quad r = \frac{r_s}{2\sqrt{3}}. \tag{3}$$

2.1.3. Projection

Inevitably, some intermediate design variables appear with the filtering process and the projection methods provide a way to obtain the black-and-white designs.

Projection for the first step: The design variable ϕ is between $[-1, 1]$; hence, the Heaviside function is employed:

$$\mu = H(\overline{\phi}) = \begin{cases} 0, & \overline{\phi} \le -h \\ 1, & \overline{\phi} \ge h \\ 0.5 + 0.9375(\overline{\phi}/h) - 0.625(\overline{\phi}/h)^3 + 0.1875(\overline{\phi}/h)^5, & -h < \overline{\phi} < h, \end{cases} \tag{4}$$

where h is the threshold for controlling the width of the smooth change of the density field from zero to one.

Projection for the second step: For the smoothed density field $\overline{\mu}$, a projection method similar to those used by Yoon and Kim (2003) and F. Wang, Lazarov, and Sigmund (2011) is used:

$$\psi = \frac{\tanh(\beta/2) + \tanh(\beta(\overline{\mu} - \eta))}{2\tanh(\beta/2)}, \tag{5}$$

where β is used to control the slope of the function and η defines the centre of the smooth transition part of the function.

2.1.4. Interpolation functions

With the density field μ and the projected smoothed density field ψ, the coating structure can be defined easily as

$$\rho_c = (1 - \mu)\psi. \tag{6}$$

Based on the Hashin–Shtrikman bounds of micro-structure (Hashin and Shtrikman 1963), the material properties of the base material are defined as a ratio of the coating material's properties:

$$\rho_b = \lambda_\rho \rho_c, \quad E_b = \lambda_E E_c, \tag{7}$$

where ρ_c and E_c are the density and Young's modulus of the coating material, and they are set to be one; ρ_b and E_b are the material properties of the base material; λ_ρ and λ_E are the ratios; and $\lambda_E \leq \lambda_\rho$ is in the interval $[0, 1]$. The base structure and the coating structure are both assumed to be isotropic with the Poisson ratio υ.

Then, the density and the Young's modulus are defined as

$$\rho(\rho_b, \rho_c) = \lambda_\rho \rho_b + \rho_c = \lambda_\rho \mu + (1 - \mu)\psi \tag{8}$$

$$E(\rho_b, \rho_c) = E[\,\lambda_E {\rho_b}^p + {\rho_c}^p] = E\{\lambda_E \mu^p + [\,(1 - \mu)\psi]^p\}, \tag{9}$$

where p is the penalization parameter, and the optimization method will push both ρ_b and ρ_c towards a zero or one solution in the design domain. In practical applications, $p = 3$ is used, and a larger penalization parameter for the base material can be used to get a clearer boundary for the uniform thickness control of the coating structure.

2.2. Optimization problem definition

The topology optimization problem that minimizes compliance to mass constraints is used to illustrate the performance of the new coating formulation. The finite element model used to solve the equilibrium equation on the domain Ω is given as follows:

$$\operatorname{div}\sigma(\mathbf{u}) + \mathbf{f_v} = 0 \quad \text{in } \Omega, \tag{10}$$

where the Cauchy stress tensor, the displacement field vector and the volume force are denoted by σ, $\mathbf{u}$ and $\mathbf{f_v}$, respectively. The Neumann and Dirichlet boundary conditions are described as follows:

$$\begin{cases} \sigma \cdot \mathbf{n} = \mathbf{f_n} & \text{on } \partial\Omega_N \\ \mathbf{u} = \mathbf{0} & \text{on } \partial\Omega_D, \end{cases} \tag{11}$$

where $\mathbf{f_n}$ and $\mathbf{n}$ define the surface traction and the unit normal vector of the boundary. The constitutive matrix is $\mathbf{C}$, and it can be formulated as

$$\sigma = \mathbf{C}\varepsilon. \tag{12}$$

After that, the topology optimization problem can be defined as follows:

$$\begin{aligned} \mathrm{Min}_{\phi} \quad & c(\phi) = \mathbf{U}^{\mathrm{T}}\mathbf{K}\mathbf{U} \\ \text{s.t.} \quad & \begin{cases} \mathbf{K}(\rho_{\mathbf{b}}, \rho_{\mathbf{c}})\mathbf{U} = \mathbf{F} \\ M(\rho_{\mathbf{b}}, \rho_{\mathbf{c}}) \leqslant \mathrm{M}^0 \\ -1 \leq \phi \leq 1. \end{cases} \end{aligned} \tag{13}$$

Here, the stiffness matrix, the displacement and the force vectors are denoted by $\mathbf{K}$, $\mathbf{U}$ and $\mathbf{F}$, respectively. The mass and the upper mass are denoted by M and M^0, respectively.

2.3. Sensitivity analysis

According to the formulation of the topology optimization, only the sensitivity of the compliance and the mass are needed for optimization. Both of them relate to the density and the Helmholtz PDE filter. The sensitivity computation of the compliance, the mass, and the filter and projection are illustrated in the following section.

2.3.1. Sensitivity of filter and projection

According to Equations (1) and (2), the sensitivity of the smoothed design variable $\overline{\phi}$ with respect to the design variable ϕ and the smoothed density field $\overline{\mu}$ with respect to the density field μ can be derived as

$$\frac{\partial \overline{\phi}}{\partial \phi} = \left[\sum \int (-\nabla N^{\mathrm{T}} R^2 \nabla N + N^{\mathrm{T}} N)\, \mathrm{d}\Omega_e\right]^{-1} \cdot \left[\sum \int N\, \mathrm{d}\Omega_e\right] \tag{14}$$

$$\frac{\partial \overline{\mu}}{\partial \mu} = \left[\sum \int (-\nabla N^{\mathrm{T}} r^2 \nabla N + N^{\mathrm{T}} N)\, \mathrm{d}\Omega_e\right]^{-1} \cdot \left[\sum \int N\, \mathrm{d}\Omega_e\right], \tag{15}$$

where N is the shape interpolation function for solving the Helmholtz PDE filter function. The detail of the derivation is described in Lazarov and Sigmund (2011).

The sensitivity of the Heaviside function equation (4) for obtaining the density field can be derived easily as

$$\frac{\partial \mu}{\partial \overline{\phi}} = \frac{\partial H(\overline{\phi})}{\partial \overline{\phi}} = \begin{cases} 0, & \overline{\phi} \leq -h \\ 0, & \overline{\phi} \geq h \\ \frac{0.9375}{h} - \frac{1.875}{h}(\overline{\phi}/h)^2 + \frac{0.9375}{h}(\overline{\phi}/h)^4, & -h < \overline{\phi} < h. \end{cases} \tag{16}$$

The sensitivity of the projection function (Equation (5)) can be derived as

$$\frac{\partial \psi}{\partial \overline{\mu}} = \frac{\beta\{1 - \tanh^2[\,\beta(\overline{\mu} - \eta)]\}}{2\tanh(\beta/2)}. \tag{17}$$

2.3.2. Sensitivity of compliance

By the adjoint method, the sensitivity of the objective with respect to the design variable ϕ can be computed as follows:

$$\frac{\mathrm{d}c}{\mathrm{d}\phi} = -\mathbf{U}^{\mathrm{T}} \frac{\partial K}{\partial \phi}\mathbf{U} = \sum_i \frac{\partial E_i}{\partial \phi}(-\mathbf{u}_i^{\mathrm{T}}\mathbf{k}^{\mathbf{0}}\mathbf{u}_i), \tag{18}$$

where E_i is the physical property. By differentiating Equation (9) with respect to ϕ, it can be detailed as

$$\frac{\partial E_i}{\partial \phi} = E\left[\lambda_E p {\rho_b}^{p-1} \frac{\partial \rho_b}{\partial \phi} + p {\rho_c}^{p-1} \frac{\partial \rho_c}{\partial \phi}\right]. \tag{19}$$

According to the definitions of the base material and coating material, and using the chain rule, $\partial\rho_b/\partial\phi$ and $\partial\rho_c/\partial\phi$ can be derived as

$$\frac{\partial\rho_b}{\partial\phi} = \frac{\partial\mu}{\partial\phi}, = \frac{\partial\mu}{\partial\overline{\phi}}\frac{\partial\overline{\phi}}{\partial\phi} \tag{20}$$

$$\frac{\partial\rho_c}{\partial\phi} = \frac{\partial(1-\mu)}{\partial\phi}\psi + (1-\mu)\frac{\partial\psi}{\partial\phi} = -\frac{\partial\mu}{\partial\phi}\psi + (1-\mu)\frac{\partial\psi}{\partial\overline{\mu}}\frac{\partial\overline{\mu}}{\partial\mu}\frac{\partial\mu}{\partial\overline{\phi}}\frac{\partial\overline{\phi}}{\partial\phi}. \tag{21}$$

2.3.3. Sensitivity of the mass constraint

The total mass is an integration of the total density field in the design domain; hence, the sensitivity can be expressed as

$$\frac{\partial M}{\partial\phi} = \sum_i \frac{\partial\rho_i}{\partial\phi} = \sum_i \left(\lambda_\rho \frac{\partial\rho_b}{\partial\phi} + \frac{\partial\rho_c}{\partial\phi}\right). \tag{22}$$

The partial differentials $\partial\rho_b/\partial\phi$ and $\partial\rho_c/\partial\phi$ have already been derived in Equations (20) and (21), respectively.

3. Optimization results

To prove the concept of the present coating filter in topology optimization, this section provides the two benchmark problems, *i.e.* cantilever and MBB beams. The penalization factors p for the base material and the coating material are set to three and the radius of the minimum length scale control is set to $R = 4r_e$, where r_e is the element size for the discretization of the design domain. The Young's modulus and the density of the coating material are set to $E = 1$ and $\rho_c = 1$, respectively. The Young's modulus ratio for the base material is set to $\lambda_E = 0.2$. The total mass constraint is set to $M^0 = 0.4$. For stable convergence, the adaptive threshold for the Heaviside function with 0.75, 0.5, 0.3 and 0.2 for the 80th, 200th and 300th iterations is used. For the projection of the second step, β is set to eight, and the continuation approach for η is employed; $\eta = 0.5$, $\eta = 0.4$, $\eta = 0.3$ and $\eta = 0.2$ are the same iterations with the Heaviside function threshold. The method of moving asymptotes (MMA) is used (Svanberg 1987). The plane strain element is used for 2D examples in the article. The thickness is set to be 20, which is more than 10 times the widths and lengths used in both the cantilever beam and the MBB beam problems.

3.1. Example 1: Cantilever beam problem

First of all, the cantilever beam ($w = 2$, $h = 1$, $f = 1$) shown in Figure 5 is solved with the present coating filter scheme. To consider the coating layer at the outer domain, the design domain discretized

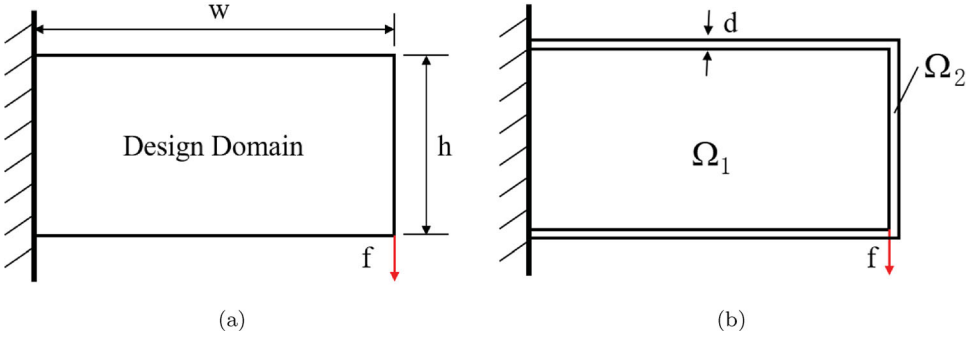

Figure 5. The cantilever example: (a) problem definition; (b) analysis model for the coating.

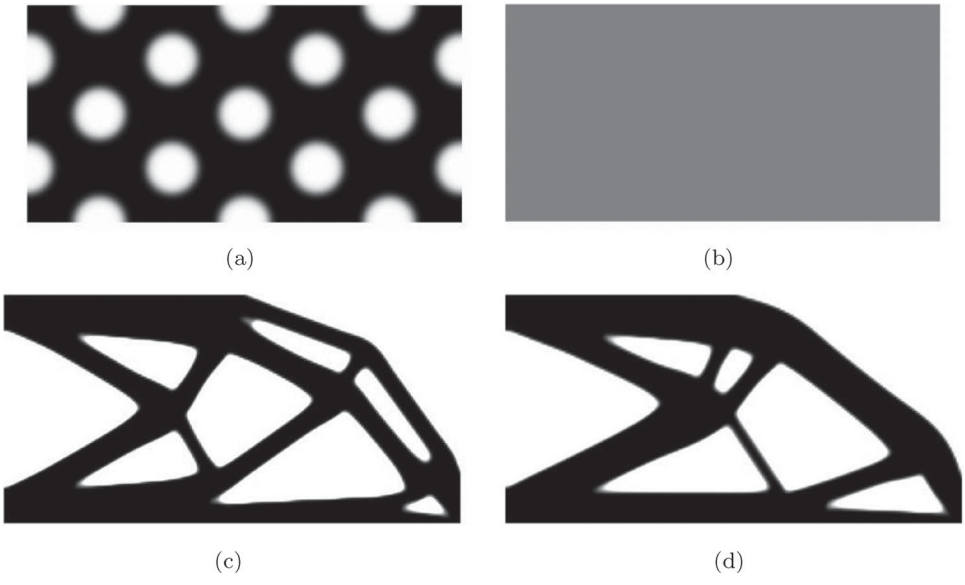

Figure 6. The topology optimization of the cantilever without coating: (a) non-uniform initialization; (b) uniform initialization; (c) the optimized design with non-uniform initialization $c = 32.650$; (d) the optimized design with uniform initialization $c = 32.344$.

with equal size square four-node element $r_e = 0.01$ is extended along the boundary with a uniform thickness $d = 0.1$, and the density of the base material is set to be $\Omega_2 = 0$.

The solid isotropic material with penalisation (SIMP) methods with non-uniform and uniform initialization are shown in Figure 6 as a comparison with the results of the coating structure with different initialization methods. Figure 6(a) shows the non-uniform initialization in which black represents the solid material and the white hole is the void material. Figure 6(b) shows the uniform initialization, where the density is set to 0.5 for every element. The optimization results are shown in Figures 6(c) and 6(d), respectively. The results of non-uniform initialization look quite different from those of uniform initialization, but with a comparable compliance of $c = 32.650$ compared with $c = 32.344$. This is because SIMP can only find a local minimum of the topology optimization problem; hence, the result may be different with different initializations.

The iteration results of the new coating model with non-uniform and uniform initialization are shown in Figures 7 and 8, respectively. The thickness control parameter is set to $r = r_e$. For the non-uniform initialization, many holes are initialized in the design domain as the void material, and the grey part is the solid material with a density of $\rho_b = 1$. Between them is the coating structure in black with coating density $\rho_c = 1$. The intermediate results with 20th, 50th, 100th, 200th and 400th iterations are shown in Figures 7(b), 7(c), 7(d), 7(e) and 7(f), respectively. It is obvious that the proposed method can easily merge coating structures. The results of coating structure optimization with uniform initialization under the same iterations are shown in Figure 8. The initialization shows that the middle part is darker than the outer boundary part; this is because the design variable is set as $\phi = 0$. Hence, the base material is $\rho_b = 0.5$ in the domain Ω_1. For the outer domain Ω_2, the base material is $\rho_b = 0$. For the coating material, the density should be $\rho_c = 0.25$ in the middle of the domain Ω_1. Near the boundary between domains Ω_1 and Ω_2, the coating material ρ_c should have a smaller value than 0.25. With this kind of uniform initialization, the intermediate optimizations with the same non-uniform initialization are shown in Figures 8(b), 8(c), 8(d), 8(e) and 8(f), respectively. It can be seen that the proposed method performs well for topology optimization of coated structures with both non-uniform and uniform initialization.

The convergence history of cantilever examples with uniform and non-uniform initialization is shown in Figure 9. The compliance is shown with a line with plus marks, and the total mass is shown

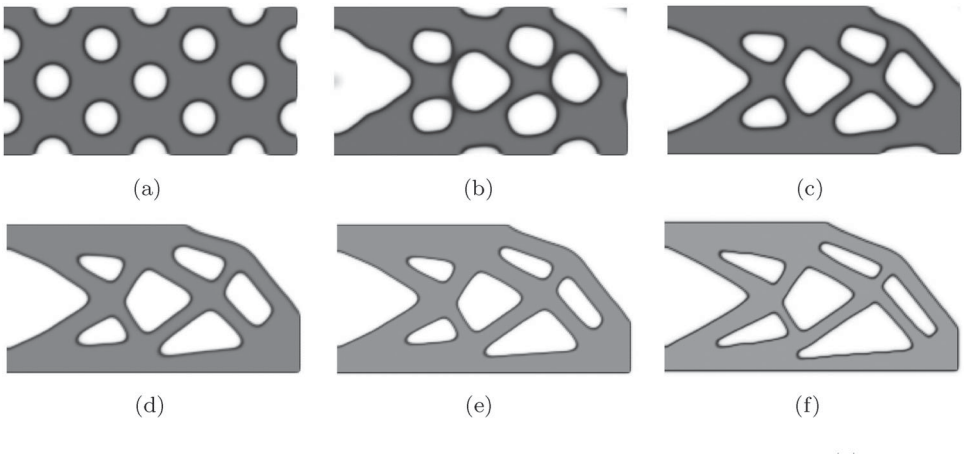

Figure 7. The iteration history of cantilever examples with non-uniform initialization: (a) 1st iteration; (b) 20th iteration; (c) 50th iteration; (d) 100th iteration; (e) 200th iteration; (f) 400th iteration.

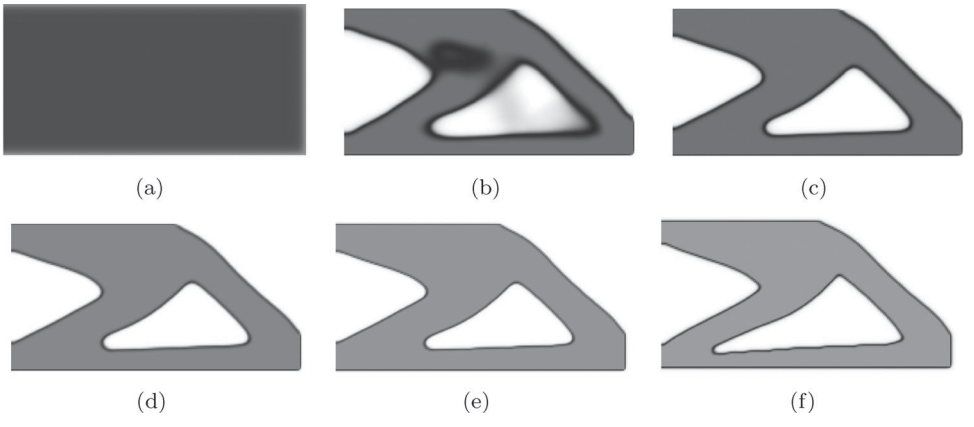

Figure 8. The iteration history of the cantilever example with uniform initialization: (a) 1st iteration; (b) 20th iteration; (c) 50th iteration; (d) 100th iteration; (e) 200th iteration; (f) 400th iteration.

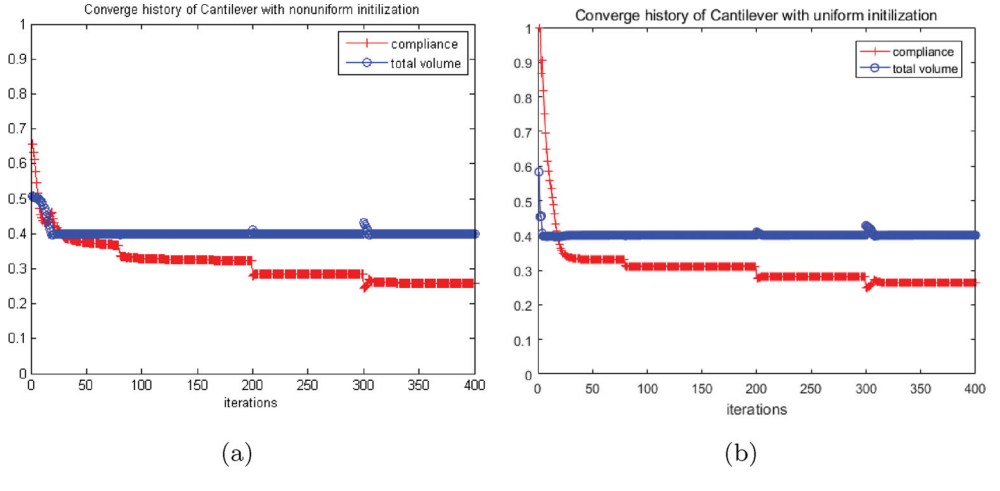

Figure 9. The convergence history of the cantilever example: (a) non-uniform initialization $c = 80.563$; (b) uniform initialization $c = 81.677$.

with a line with circle marks. The compliance is normalized with the result of uniform initialization for the compliance being much larger than that of non-uniform initialization. It can be seen that the mass drops dramatically for uniform initialization, and thus the compliance does as well. However, for the non-uniform initialization, it takes about 20 iterations to meet the mass constraint, and the compliance has vibrations during optimization due to the merging of holes. During the optimization of both uniform and non-uniform initialization, there is a small step change in the compliance due to the use of smaller thresholds for the projections at the 80th, 200th and 300th iterations. This is the same as the mass constraint. However, the results show that both the compliance and mass constraint would converge appropriately even with these discontinuous changes.

The results of coating structure modelling with the thickness control parameters $r = r_e$ and $r = 2r_e$ are shown in Figures 10, 11, 12 and 13, respectively. It can be seen that, with a low base material density $\lambda_\rho = 0.5$, the optimized shapes are almost the same with uniform and non-uniform initialization, and so is the compliance. By increasing the thickness of the coating material, the compliance reduces by more than 10%, and there is a slight change in the shape. With the same coating structure thickness,

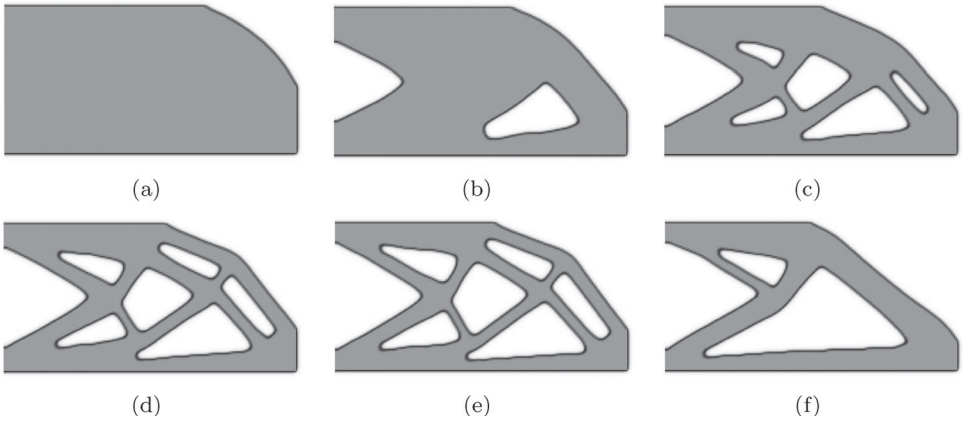

Figure 10. Cantilever examples with different base material densities for the coating at a radius of $r = 1$ with non-uniform initialization: (a) base density $\rho = 0.5$, $c = 59.766$; (b) base density $\rho = 0.6$, $c = 66.099$; (c) base density $\rho = 0.7$, $c = 73.458$; (d) base density $\rho = 0.8$, $c = 80.563$; (e) base density $\rho = 0.9$, $c = 87.451$; (f) base density $\rho = 0.95$, $c = 93.961$.

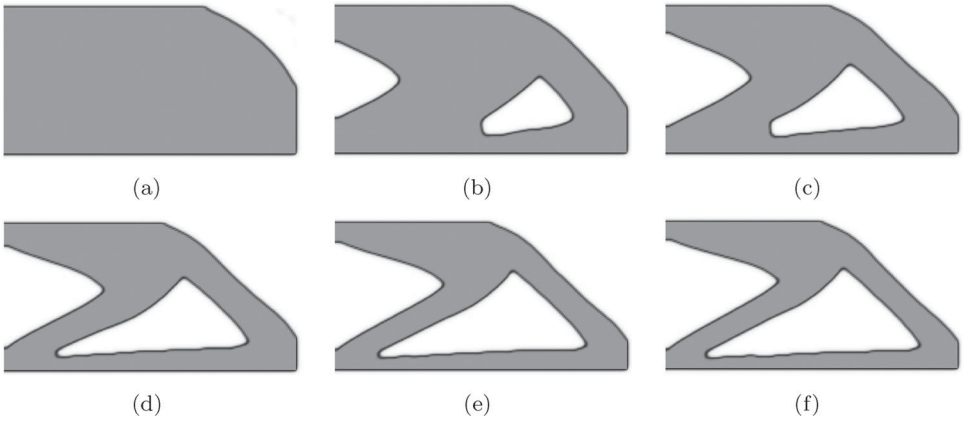

Figure 11. Cantilever examples with different base material densities for the coating at a radius of $r = 1$ with uniform initialization: (a) base density $\rho = 0.5$, $c = 59.778$; (b) base density $\rho = 0.6$, $c = 66.118$; (c) base density $\rho = 0.7$, $c = 74.046$; (d) base density $\rho = 0.8$, $c = 81.677$; (e) base density $\rho = 0.9$, $c = 89.579$; (f) base density $\rho = 0.95$, $c = 93.03$.

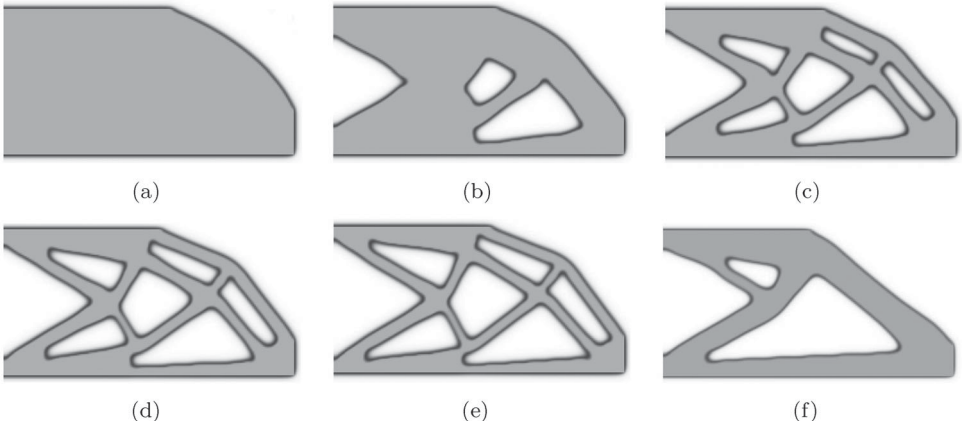

Figure 12. Cantilever examples with different base material densities for the coating at a radius of $r = 2$ with non-uniform initialization: (a) base density $\rho = 0.5, c = 54.430$; (b) base density $\rho = 0.6, c = 59.765$; (c) base density $\rho = 0.7, c = 64.657$; (d) base density $\rho = 0.8, c = 69.315$; (e) base density $\rho = 0.9, c = 74.032$; (f) base density $\rho = 0.95, c = 93.282$.

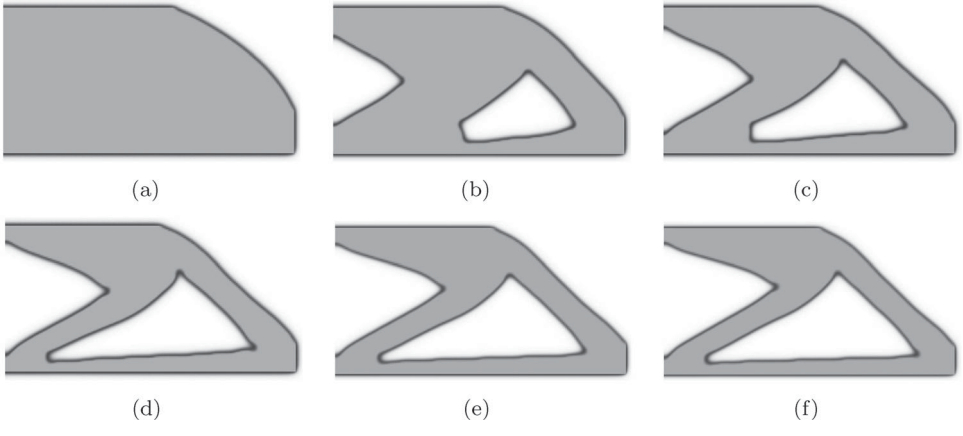

Figure 13. Cantilever examples with different base material densities for the coating at a radius of $r = 2$ with uniform initialization: (a) base density $\rho = 0.5, c = 54.436$; (b) base density $\rho = 0.6, c = 59.916$; (c) base density $\rho = 0.7, c = 63.991$; (d) base density $\rho = 0.8, c = 71.484$; (e) base density $\rho = 0.9, c = 84.154$; (f) base density $\rho = 0.95, c = 91.665$

the results of coating structure optimization change quite a lot when the density of the base material is increased from $\rho_b = 0.5$ to $\rho_b = 0.95$ with non-uniform initialization, as shown in Figures 10 and 12. The results of uniform initialization are shown in Figures 11 and 13, which show that the optimized shape looks similar. The compliance of the optimized shapes shown in Figures 10, 11, 12 and 13 is comparable even though the shapes differ quite a lot. One thing that needs to be mentioned is that the result for a base material density of $\rho_b = 0.95$ totally differs from the others, as more holes are merged because it cannot make the coating with six holes in the middle any thicker. However, the shape of the optimization result of the uniform initialization is similar at this local minimum. It has a simple topology, which is difficult to change to other shapes. However, the compliance levels of the uniform and non-uniform initialization are also comparable because both of them are local minima.

3.2. Example 2: The Messerschmitt–Bölkow–Blohm beam problem

The MBB beam is used as another example to illustrate the performance of coating structure optimization, as shown in Figure 14(a). The design domain is a rectangular area of unit thickness with

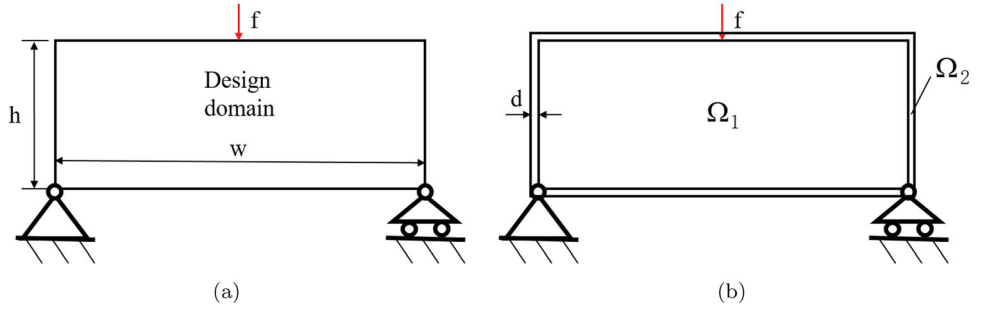

Figure 14. The MBB beam example: (a) problem definition; and (b) analysis model for coating.

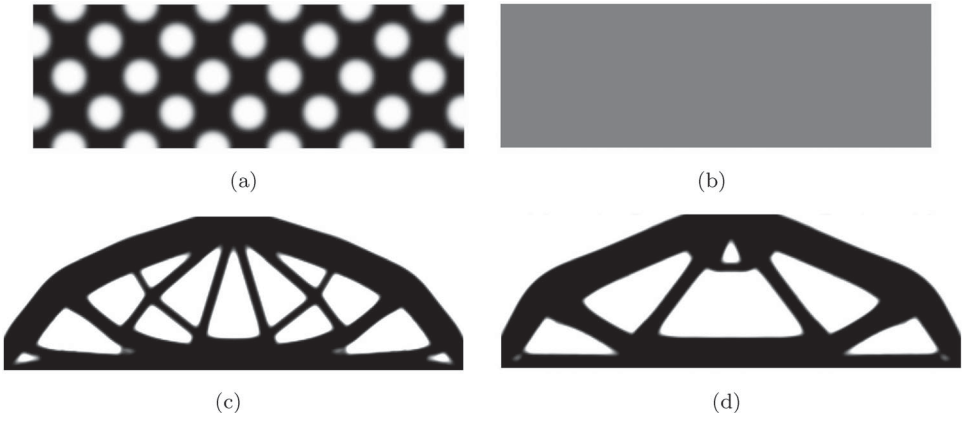

Figure 15. Topology optimization of the MBB beam without coating: (a) non-uniform initialization; (b) uniform initialization; (c) the optimized design with non-uniform initialization $c = 10.890$; (d) the optimized design with uniform initialization $c = 10.881$.

$w = 3$ and $h = 1$, and it is simply supported on the left and right lower corners. A concentrated load of $f = 1$ is applied to the middle of the top surface of the rectangle. The rectangle is extended along the boundary of thickness $d = 0.1$ to construct the analysis model for the coating structure, as shown in Figure 14(b). As was defined in the analysis model of the cantilever example, the density of the base material in the extended domain is set to be $\Omega_2 = 0$, and the design domain is discretized with an equal-sized, square, four-node element $r_e = 0.01$.

Topology optimization of the MBB beam by the SIMP method with uniform and non-uniform initialization is shown in Figure 15. The total mass constraint is 40% of the domain with solid coating materials. The non-uniform initialization creates many holes in the design domain with the solid material. The uniform initialization starts with a base density of 0.5. The optimized results are shown in Figures 15(c) and 15(d), respectively. The optimized shape looks quite different, but the compliance levels are comparable with $c = 10.890$ and $c = 10.881$ for non-uniform and uniform initialization, respectively.

A comparison is conducted of the conventional method (Clausen, Aage, and Sigmund 2015) and the proposed method for the topology optimization of coated structures with the MBB beam example. The coating thickness is set to be $r = 2r_e$, and the density of the base material to be $\rho = 0.65$. Both the present method and the conventional method result in appropriate coating structures covering the surface of the base material, as shown in Figure 16. The optimized coating structure prepared by the present method and by the conventional method look quite similar, except for the holes in the middle bottom of the optimized structure and the shape of the holes; the compliance levels are $c = 20.606$ and $c = 21.659$, respectively, and they are comparable. The details for the optimized coating structure

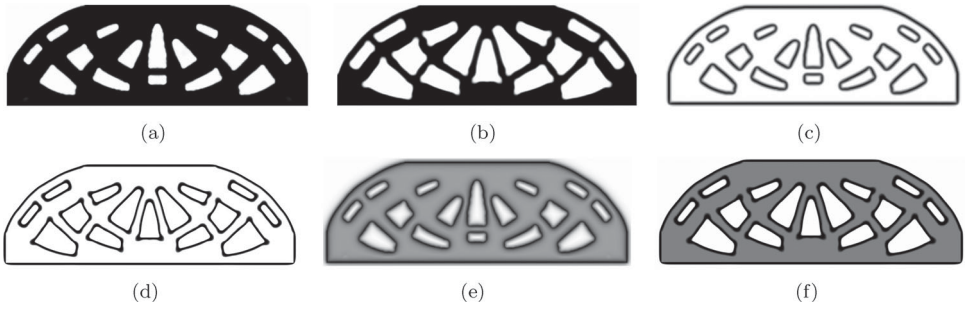

Figure 16. Comparison of the conventional method (Clausen, Aage, and Sigmund 2015) $c = 21.659$ and the proposed method $c = 20.606$ for topology optimization of coated structures with the MBB beam example: (a) base material of the conventional method; (b) base material of the present method; (c) coating material of the conventional method; (d) coating material of the present method; (e) optimized structure of the conventional method; (f) optimized structure of the present method.

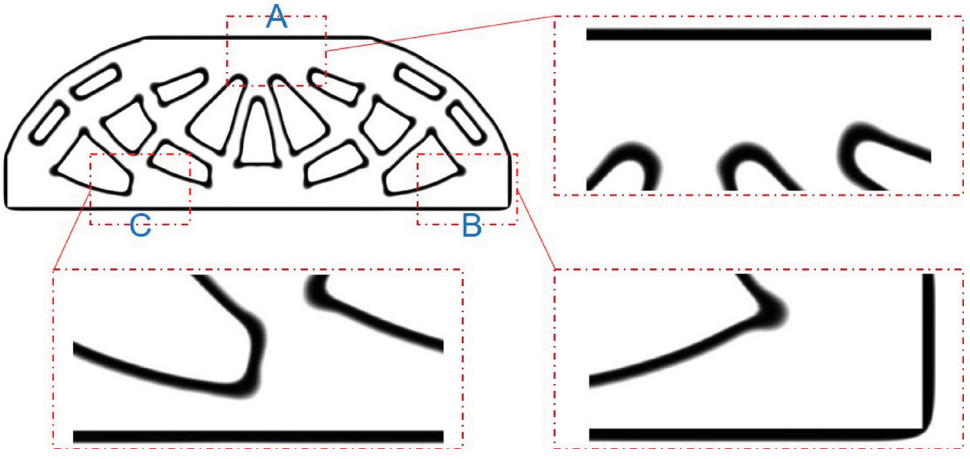

Figure 17. Details of optimized coated structures prepared by the present method.

by the proposed method are shown in Figure 17. It can be seen that the optimized coating structure is almost uniform except for the corners, which is reasonable because exact zero/one values for the base material cannot be obtained at these points, even with a very large projection parameter.

The influences of the density of the base material and the thickness of the coating material are also determined for the MBB beam example. By setting the coating thickness to be $r = r_e$, it creates holes in low density base materials $\lambda_\rho = 0.55$ with non-uniform initialization, while a simple shape for the uniform initialization. However, the compliance is comparable. The optimized shapes still change quite a lot for non-uniform initialization, while those of the uniform initialization have similar shapes, except for that of the base material density $\lambda_\rho = 0.95$. The structure stiffness reduces more compared with shapes under non-uniform initialization. This is because, under uniform initialization, the middle bar of $\lambda_\rho = 0.9$ cannot become any thinner due to the minimum length scale constraint of $R = 4r_e$. However, the optimized coating structures are still comparable with uniform and non-uniform initialization, as shown in Figures 18 and 19.

As the coating thickness reaches $r = 2r_e$, the optimization method finds a simple topology shape with uniform initialization, while non-uniform initialization results in complex topology. The compliance of the results drops by about 20% compared with the one with a coating thickness of $r = 0.5r_e$, and the optimized shape totally changes, as shown in Figures 20 and 21. This is because the coating

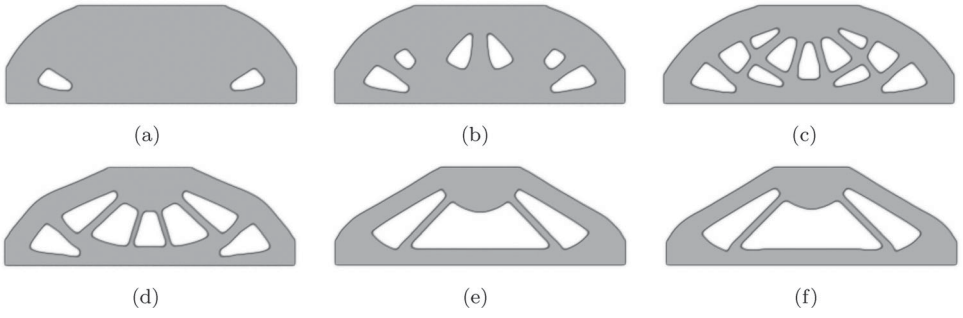

Figure 18. The MBB beam example with different base material densities for the coating at a radius of $r = 1$ with non-uniform initialization: (a) base density $\rho = 0.55$, $c = 20.084$; (b) base density $\rho = 0.6$, $c = 21.341$; (c) base density $\rho = 0.7$, $c = 23.515$; (d) base density $\rho = 0.8$, $c = 25.985$; (e) base density $\rho = 0.9$, $c = 28.721$; (f) base density $\rho = 0.95$, $c = 29.935$.

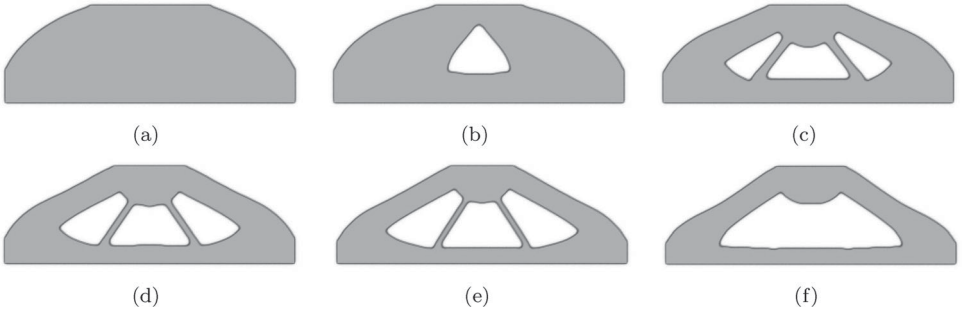

Figure 19. The MBB beam example with different base material densities for the coating at a radius of $r = 1$ with uniform initialization: (a) base density $\rho = 0.55$, $c = 20.012$; (b) base density $\rho = 0.6$, $c = 21.487$; (c) base density $\rho = 0.7$, $c = 23.860$; (d) base density $\rho = 0.8$, $c = 26.285$; (e) base density $\rho = 0.9$, $c = 28.832$; (f) base density $\rho = 0.95$, $c = 31.070$.

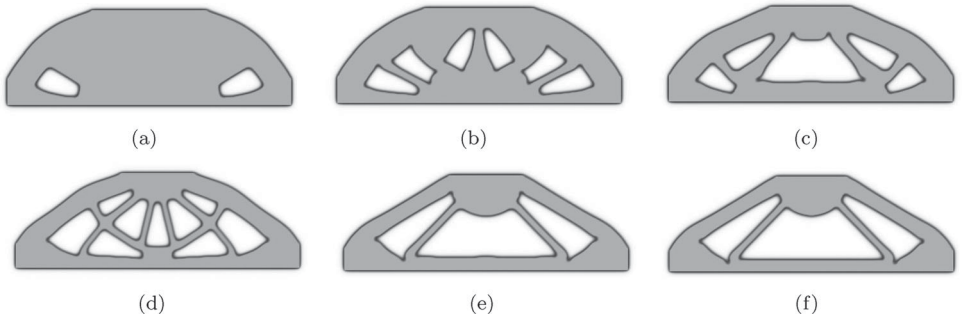

Figure 20. The MBB beam example with different base material densities for the coating at a radius of $r = 2$ with non-uniform initialization: (a) base density $\rho = 0.55$, $c = 17.963$; (b) base density $\rho = 0.6$, $c = 18.988$; (c) base density $\rho = 0.7$, $c = 21.029$; (d) base density $\rho = 0.8$, $c = 23.480$; (e) base density $\rho = 0.9$, $c = 24.505$; (f) base density $\rho = 0.95$, $c = 25.256$.

structure contributes much more to the structure stiffness, which drives the optimization into different local minima with the same mass constraint. With a thick coating structure, the compliance is still comparable for non-uniform and uniform initialization, though the optimized shapes are quite different. This is because the coating structure will make the object function more complex; thus, there will be more comparable local minima in the design domain.

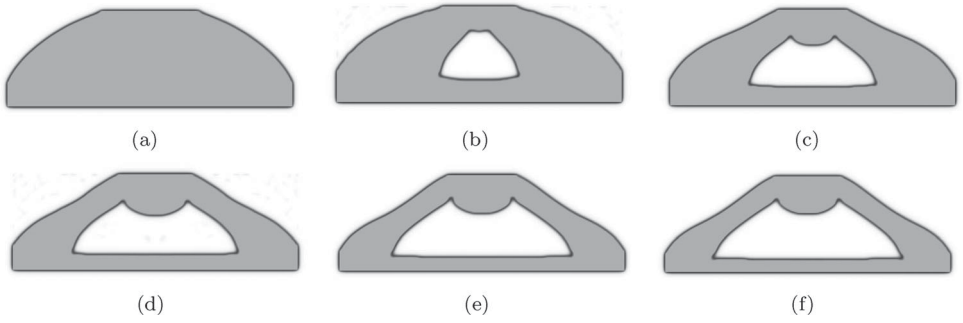

Figure 21. The MBB beam example with different base material densities for the coating at a radius of $r = 2$ with uniform initialization: (a) base density $\rho = 0.55, c = 18.222$; (b) base density $\rho = 0.6, c = 19.464$; (c) base density $\rho = 0.7, c = 21.783$; (d) base density $\rho = 0.8, c = 24.112$; (e) base density $\rho = 0.9, c = 25.685$; (f) base density $\rho = 0.95, c = 26.552$.

4. Conclusions

This research article developed a new schema for coating structure optimization by combining the filtering-projected density field and the original density field variables for general meshes. Similar to conventional coating modelling (Clausen, Aage, and Sigmund 2015), the proposed coating schema also contains two steps, filtering and projection, but the filtering and projection of the density field are employed in the second step instead of the gradient norm. This avoids the complex computing of the gradient and the inexact approximation of the maximum gradient norm. The proposed method also has the advantage of containing both the base material and coating material variables in the design domain. It has the ability to change smoothly from both void and base materials to the coating; hence, it can merge isolated coating structures easily when needed.

Several numeral examples were solved to illustrate the performance of the proposed coating structure model. Both non-uniform and uniform initialization were conducted to show the ability of the proposed method to perform coating optimization. The optimized results of the non-uniform initialization provided the advantages of coating structure merging and new coating creation in the base material domain. The results also show that non-uniform initialization and uniform initialization can obtain comparable results with quite different shapes, as the coating structure makes the objective function more complex, so there will be many local minima. Coating structures with different thicknesses and base material densities under the same physical properties and mass constraints were also developed in the article. It was found that the thickness and the density of the base material had big influences on the optimization of the coating structure. The 3D coated example also showed the efficiency and effectiveness of the new coating method for large-scale topology optimization problems with 3D structures.

We expect that future work will involve the use of a buckling constraint for coating structure optimization. Moreover, the coating schema could be applied for 3D printing manufacturing with improvements in both the structure stiffness and buckling stability, and also considering manufacturing constraints, which would be especially valuable. Because an additional filtering operation has been introduced to formulate the coating structure, obviously causing the topology optimization problem to become more non-convex and have more local optima, the research herein could be extended to eliminate the probability of being trapped in local optima (Gao, Li, and Ma 2017; Rojas-Labanda and Stolpe 2015; Li and Khandelwal 2015).

Disclosure statement

No potential conflict of interest was reported by the author(s).

Funding

The financial supports were provided by the National Natural Science Foundation of China [grant number 51975589]; the Natural Science Foundation of Hunan Province [grant number 2018JJ3663]. These sources of support are gratefully acknowledged.

References

Allaire, Grégoire, François Jouve, and Anca-Maria Toader. 2004. "Structural Optimization Using Sensitivity Analysis and a Level-Set Method." *Journal of Computational Physics* 194 (1): 363–393. doi:10.1016/j.jcp.2003.09.032

Bendsøe, Martin Philip, and Noboru Kikuchi. 1988. "Generating Optimal Topologies in Structural Design Using a Homogenization Method." *Computer Methods in Applied Mechanics and Engineering* 71 (2): 197–224. doi:10.1016/0045-7825(88)90086-2

Clausen, Anders, Niels Aage, and Ole Sigmund. 2015. "Topology Optimization of Coated Structures and Material Interface Problems." *Computer Methods in Applied Mechanics and Engineering* 290: 524–541. doi:10.1016/j.cma.2015.02.011

Clausen, Anders, Niels Aage, and Ole Sigmund. 2016. "Exploiting Additive Manufacturing Infill in Topology Optimization for Improved Buckling Load." *Engineering* 2 (2): 250–257. doi:10.1016/J.ENG.2016.02.006

Fu, Junjian, Hao Li, Liang Gao, and Mi Xiao. 2019. "Design of Shell-Infill Structures by a Multiscale Level Set Topology Optimization Method." *Computers & Structures* 212: 162–172. doi:10.1016/j.compstruc.2018.10.006

Fu, Junjian, Hao Li, Mi Xiao, Liang Gao, and Sheng Chu. 2019. "Topology Optimization of Shell-Infill Structures Using a Distance Regularized Parametric Level-Set Method." *Structural and Multidisciplinary Optimization* 59 (1): 249–262. doi:10.1007/s00158-018-2064-6

Gao, Xingjun, Lijuan Li, and Haitao Ma. 2017. "An Adaptive Continuation Method for Topology Optimization of Continuum Structures Considering Buckling Constraints." *International Journal of Applied Mechanics* 9 (7): Article ID 1750092. doi:10.1142/S1758825117500922

Guest, J. K., J. H. Prévost, and T. Belytschko. 2014. "Achieving Minimum Length Scale in Topology Optimization Using Nodal Design Variables and Projection Functions." *International Journal for Numerical Methods in Engineering* 61 (2): 238–254. doi:10.1002/nme.1064

Hashin, Z., and S. Shtrikman. 1963. "A Variational Approach to the Theory of the Elastic Behaviour of Multiphase Materials." *Journal of the Mechanics and Physics of Solids* 11 (2): 127–140. doi:10.1016/0022-5096(63)90060-7

Kawamoto, Atsushi, Tadayoshi Matsumori, Shintaro Yamasaki, Tsuyoshi Nomura, Tsuguo Kondoh, and Shinji Nishiwaki. 2011. "Heaviside Projection Based Topology Optimization by a PDE-Filtered Scalar Function." *Structural and Multidisciplinary Optimization* 44 (1): 19–24. doi:10.1007/s00158-010-0562-2

Lazarov, B. S., and O. Sigmund. 2011. "Filters in Topology Optimization Based on Helmholtz-Type Differential Equations." *International Journal for Numerical Methods in Engineering* 86 (6): 765–781. doi:10.1002/nme.3072

Li, Lei, and Kapil Khandelwal. 2015. "Volume Preserving Projection Filters and Continuation Methods in Topology Optimization." *Engineering Structures* 85: 144–161. doi:10.1016/j.engstruct.2014.10.052

Liu, Shutian, Quhao Li, Junhuan Liu, Wenjiong Chen, and Yongcun Zhang. 2018. "A Realization Method for Transforming a Topology Optimization Design Into Additive Manufacturing Structures." *Engineering* 4 (2): 277–285. doi:10.1016/j.eng.2017.09.002

Lu, Lin, Andrei Sharf, Haisen Zhao, Yuan Wei, Qingnan Fan, Xuelin Chen, Yann Savoye, *et al.* 2014. "Build-to-Last: Strength to Weight 3D Printed Objects." *ACM SIGGRAPH* 33 (4): 97:1–97:10. https://homes.cs.washington.edu/haisen/BuildtoLast/index.html

Møller, Per, and Lars Pleth Nielsen. 2013. *Advanced Surface Technology: A Holistic View on the Extensive and Intertwined World of Applied Surface Engineering*. Washington, DC: Møller & Nielsen; NASF.

Peng, Xiang, Tianji Wu, Jiquan Li, Shaofei Jiang, Chan Qiu, and Bing Yi. 2018. "Hybrid Reliability Analysis with Uncertain Statistical Variables, Sparse Variables and Interval Variables." *Engineering Optimization* 50 (8): 1347–1363. doi:10.1080/0305215X.2017.1400025

Rojas-Labanda, Susana, and Mathias Stolpe. 2015. "Automatic Penalty Continuation in Structural Topology Optimization." *Structural and Multidisciplinary Optimization* 52 (06): 1205–1221. doi:10.1007/s00158-015-1277-1

Schaedler, T. A., A. J. Jacobsen, A. Torrents, A. E. Sorensen, J. Lian, J. R. Greer, L. Valdevit, and W. B. Carter. 2011. "Ultralight Metallic Microlattices." *Science* 334 (6058): 962–965. doi:10.1126/science.1211649

Shchukin, Dmitry, and Helmuth Möhwald. 2013. "A Coat of Many Functions." *Science* 341 (6153): 1458–1459. doi:10.1126/science.1242895

Sigmund, Ole, and Kurt Maute. 2013. "Topology Optimization Approaches." *Structural and Multidisciplinary Optimization* 48 (6): 1031–1055. doi:10.1007/s00158-013-0978-6

Svanberg, Krister. 1987. "The Method of Moving Asymptotes—A New Method for Structural Optimization." *International Journal for Numerical Methods in Engineering* 24 (2): 359–373. doi:10.1002/nme.1620240207

Syed, A. M. Tofail, Elias P. Koumoulos, Amit Bandyopadhyay, Susmita Bose, Lisa O'Donoghue, and Costas Charitidis. 2018. "Additive Manufacturing: Scientific and Technological Challenges, Market Uptake and Opportunities." *Materials Today* 21 (1): 22–37. doi:10.1016/j.mattod.2017.07.001

Wang, Yu, Dezheng Hu, Hailin Wang, Tinghao Zhang, and Hao Yan. 2020. "Practical Design Optimization of Cellular Structures for Additive Manufacturing." *Engineering Optimization* 52 (11): 1887–1902. doi:10.1080/0305215X.2019.1696785

Wang, Yaguang, and Zhan Kang. 2018. "A Level Set Method for Shape and Topology Optimization of Coated Structures." *Computer Methods in Applied Mechanics and Engineering* 329: 553–574. doi:10.1016/j.cma.2017.09.017

Wang, Fengwen, Boyan Stefanov Lazarov, and Ole Sigmund. 2011. "On Projection Methods, Convergence and Robust Formulations in Topology Optimization." *Structural and Multidisciplinary Optimization* 43 (6): 767–784. doi:10.1007/s00158-010-0602-y

Wang, Michael Yu, Xiaoming Wang, and Dongming Guo. 2003. "A Level Set Method for Structural Topology Optimization." *Computer Methods in Applied Mechanics and Engineering* 192 (1): 227–246. doi:10.1016/S0045-7825(02)00559-5

Wang, Weiming, Tuanfeng Y. Wang, Zhouwang Yang, Ligang Liu, Xin Tong, Weihua Tong, Jiansong Deng, *et al.* 2013. "Cost-Effective Printing of 3D Objects with Skin–Frame Structures." *ACM Transactions on Graphics* 32 (6): Article No. 177. doi:10.1145/2508363.2508382

Wu, Jun, Niels Aage, R. Westermann, and Ole Sigmund. 2018. "Infill Optimization for Additive Manufacturing—Approaching Bone-Like Porous Structures." *IEEE Transactions on Visualization and Computer Graphics* 24 (2): 1127–1140. doi:10.1109/TVCG.2017.2655523

Wu, Jun, Anders Clausen, and Ole Sigmund. 2017. "Minimum Compliance Topology Optimization of Shell-Infill Composites for Additive Manufacturing." *Computer Methods in Applied Mechanics and Engineering* 326: 358–375. doi:10.1016/j.cma.2017.08.018

Xie, Y. M., and G. P. Steven. 1993. "A Simple Evolutionary Procedure for Structural Optimization." *Computers & Structures* 49 (5): 885–896. doi:10.1016/0045-7949(93)90035-C

Yi, Bing, Yuqing Zhou, Gil Ho Yoon, and Kazuhiro Saitou. 2019. "Topology Optimization of Functionally-Graded Lattice Structures with Buckling Constraints." *Computer Methods in Applied Mechanics and Engineering* 354: 593–619. doi:10.1016/j.cma.2019.05.055

Yoon, Gil Ho, and Yoon Young Kim. 2003. "The Role of S-Shape Mapping Functions in the SIMP Approach for Topology Optimization." *KSME International Journal* 17 (10): 1496–1506. doi:10.1007/BF02982329

Yoon, Gil Ho, and Bing Yi. 2019. "A New Coating Filter of Coated Structure for Topology Optimization." *Structural and Multidisciplinary Optimization* 60: 1527–1544. doi:10.1007/s00158-019-02279-7

Appendix. Example 3—3D example

Finally, the 3D cantilever beam with $w = 2, h = 1$ and $l = 1$, where l is the depth of the extrusion of the 2D cantilever along the axis perpendicular to the plane, is solved with the present coating filter scheme. The force $f = 1$ is applied to the left part, and the freedom of the right surface is constrained. The design domain is extended along the top, bottom, front and back surfaces with a uniform thickness of $d = 0.1$, and the density of the base material is set to $\Omega_2 = 0$. The design domain discretized with equal-sized, cubed, eight-node elements $r_e = 0.1$ and $r_e = 0.05$ is used to test the performance of the proposed method. The density ratio of the base material is set to $\rho_b = 0.9$. The minimum length scale control parameter is set to $R = 0.5r_e$, and the thickness control parameter of the coated structure is set to $r = r_e$.

Figures A1 and A2 show the results for the topology optimization of the 3D coating of the cantilever beams with coarse mesh $r_e = 0.1$ and fine mesh $r_e = 0.05$, respectively. The optimized base structure and coated structure are shown in Figures A1, A2(a) and A2(b). It can be seen that the coated material covers the base material exactly, and the proposed method assigns a coated structure near the periphery of the optimized structure, which greatly improves the structure's stiffness. The compliance is $c = 43.180$ and $c = 47.290$ for the coarse mesh and fine mesh, respectively. In the middle of the base material structures, there are isolated structures for coarse mesh, but they are perfectly covered by the coated structure, as shown by the parallel slices of base material and coated material in Figures A1(c) and A1(d). However, the structures for the fine mesh are similar to parallel wall structures; hence, the coated material has a similar wall structure to cover all of the base structures. Although the topology of the cross-section of the coated structures changes dramatically, the structures are all connected without an isolated coated structure, which is different from the 2D cantilever example. Hence, the optimized structure with a connected coated structure covering the base structure could have greatly improved performance with a low stiffness-to-weight ratio.

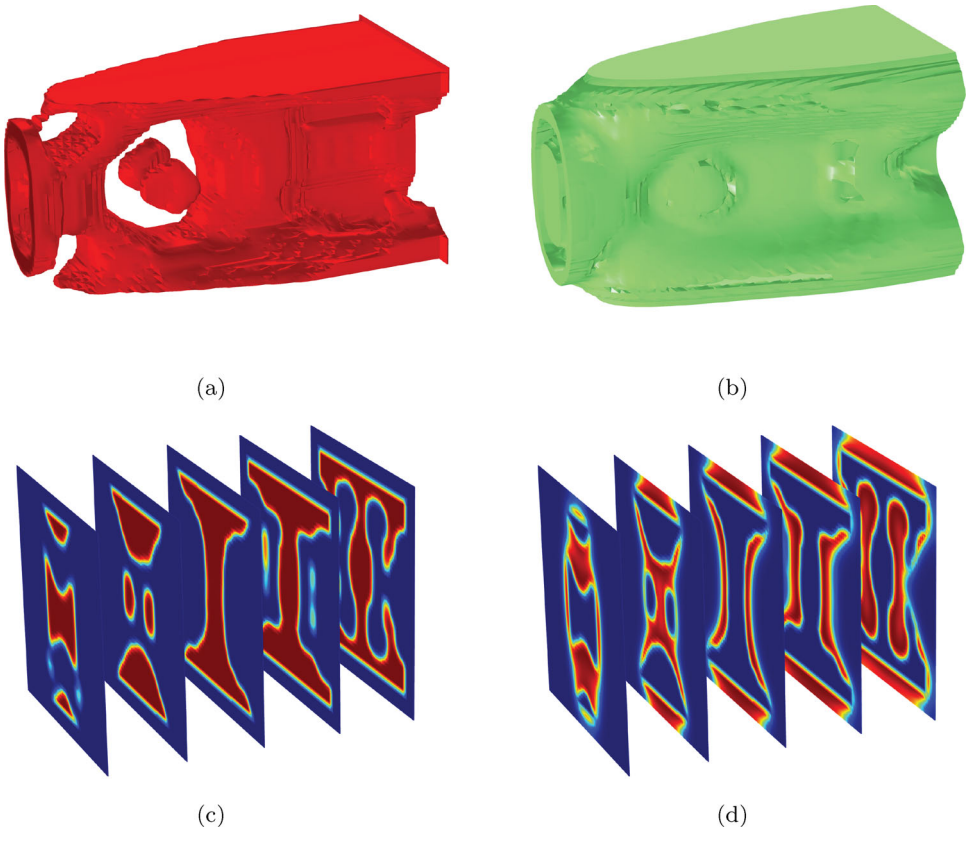

Figure A1. Three-dimensional coating for the cantilever with coarse mesh $c = 43.180$: (a) base material; (b) coated material; (c) parallel slices of base material; (d) parallel slices of coated material. (For interpretation of the references to colour in this figure, the reader is referred to the web version of this article.)

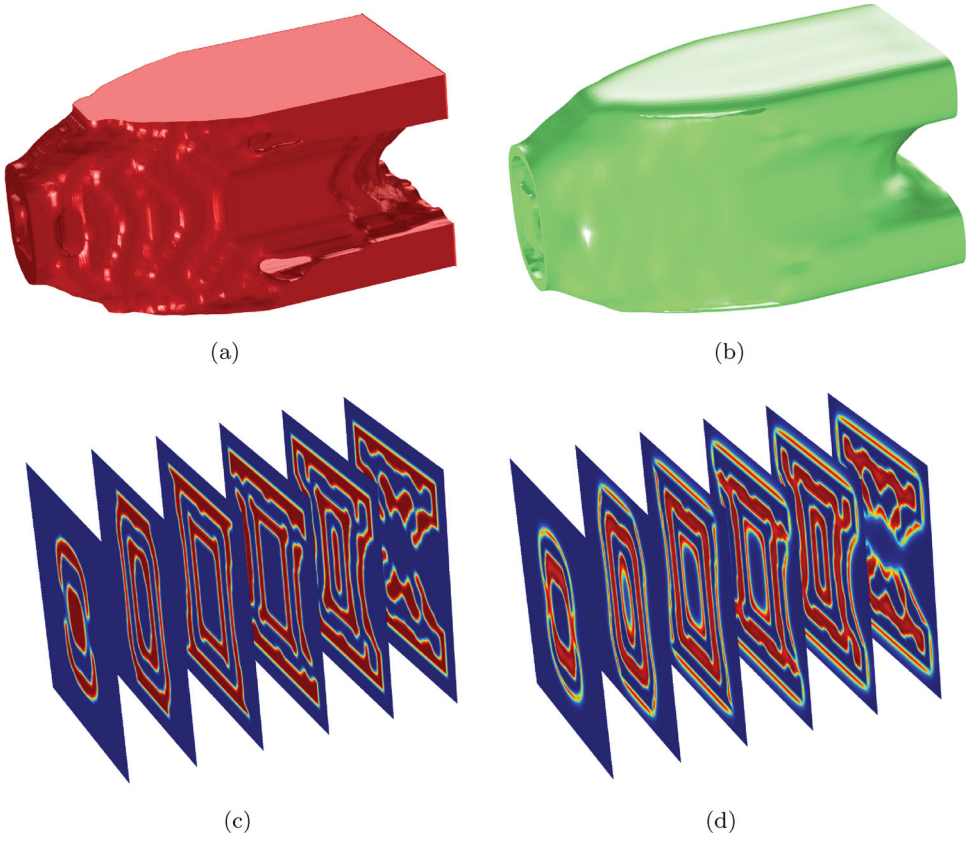

Figure A2. Three-dimensional coating for the cantilever with fine mesh $c = 47.290$: (a) base material; (b) coated material; (c) parallel slices of base material; (d) parallel slices of coated material (For interpretation of the references to colour in this figure, the reader is referred to the web version of this article.)